FOR FURTHER TRANSMITTAL

APPROVED FOR PUBLIC RELEASE, DISTRIBUTION UNLIMITED

(14) TI-ALEX(01)-TR-77-03

(6)

THE DEFLECTION DETECTOR - ITS THEORY AND EVALUATION ON SHORT-PERIOD SEISMIC DATA

(12)

(9) TECHNICAL REPORT NO. 3

VELA NETWORK EVALUATION AND AUTOMATIC PROCESSING RESEARCH

Prepared by

(10) Mark J. Shensa

TEXAS INSTRUMENTS INCORPORATED
Equipment Group
Post Office Box 6015
Dallas, Texas 75222

Prepared for

AIR FORCE TECHNICAL APPLICATIONS CENTER
Alexandria, Virginia 22314

AD A055248

AD No. DDC FILE COPY

DDC RECEIVED JUN 16 1978 E

Sponsored by

ADVANCED RESEARCH PROJECTS AGENCY
Nuclear Monitoring Research Office
ARPA Program Code No. 7F10
ARPA Order No. 2551

(11) 2 November 1977 (12) 55 p.

Acknowledgment: This research was supported by the Advanced Research Projects Agency, Nuclear Monitoring Research Office, under Project VELA-UNIFORM, and accomplished under the technical direction of the Air Force Technical Applications Center under Contract Number (15) F08606-77-C-0004,

ARPA Order-2551

18 06 13 109

405 076

APPROVED FOR PUBLIC RELEASE, DISTRIBUTION UNLIMITED

ALEX(01)-TR-77-03

THE DEFLECTION DETECTOR - ITS THEORY AND EVALUATION ON SHORT-PERIOD SEISMIC DATA

TECHNICAL REPORT NO. 3

VELA NETWORK EVALUATION AND AUTOMATIC PROCESSING RESEARCH

Prepared by
Mark J. Shensa

TEXAS INSTRUMENTS INCORPORATED
Equipment Group
Post Office Box 6015
Dallas, Texas 75222

Prepared for

AIR FORCE TECHNICAL APPLICATIONS CENTER
Alexandria, Virginia 22314

Sponsored by

ADVANCED RESEARCH PROJECTS AGENCY
Nuclear Monitoring Research Office
ARPA Program Code No. 7F10
ARPA Order No. 2551

2 November 1977

Acknowledgment: This research was supported by the Advanced Research Projects Agency, Nuclear Monitoring Research Office, under Project VELA-UNIFORM, and accomplished under the technical direction of the Air Force Technical Applications Center under Contract Number F08606-77-C-0004.

78 06 13 109

UNCLASSIFIED

SECURITY CLASSIFICATION OF THIS PAGE (When Data Entered)

REPORT DOCUMENTATION PAGE		READ INSTRUCTIONS BEFORE COMPLETING FORM
1. REPORT NUMBER	2. GOVT ACCESSION NO.	3. RECIPIENT'S CATALOG NUMBER
4. TITLE (and Subtitle) THE DEFLECTION DETECTOR - ITS THEORY AND EVALUATION ON SHORT-PERIOD SEISMIC DATA		5. TYPE OF REPORT & PERIOD COVERED Technical
		6. PERFORMING ORG. REPORT NUMBER ALEX(01)-TR-77-03
7. AUTHOR(s) Mark J. Shensa		8. CONTRACT OR GRANT NUMBER(s) F08606-77-C-0004
9. PERFORMING ORGANIZATION NAME AND ADDRESS Texas Instruments Incorporated Equipment Group Dallas, Texas 75222		10. PROGRAM ELEMENT, PROJECT, TASK AREA & WORK UNIT NUMBERS VELA T/7705/B/ETR
11. CONTROLLING OFFICE NAME AND ADDRESS Advanced Research Projects Agency Nuclear Monitoring Research Office Arlington, Virginia 22209		12. REPORT DATE 2 November 1977 13. NUMBER OF PAGES 53
14. MONITORING AGENCY NAME & ADDRESS (if different from Controlling Office) Air Force Technical Applications Center VELA Seismological Center Alexandria, Virginia 22314		15. SECURITY CLASS. (of this report) UNCLASSIFIED 15a. DECLASSIFICATION/DOWNGRADING SCHEDULE

16. DISTRIBUTION STATEMENT (of this Report)

APPROVED FOR PUBLIC RELEASE, DISTRIBUTION UNLIMITED

17. DISTRIBUTION STATEMENT (of the abstract entered in Block 20, if different from Report)

18. SUPPLEMENTARY NOTES

ARPA Order No. 2551

19. KEY WORDS (Continue on reverse side if necessary and identify by block number)

Eckhart deflection criterion
seismic noise
seismic spectra
exponential average
detector
seismic
deflection

ABSTRACT

20. ABSTRACT (Continue on reverse side if necessary and identify by block number)

This study investigates the application of a deflection detector to short-period seismic data. In general, for power detectors, no single filter will be optimal for a large variety of signals in a dynamic noise environment. The deflection detector represents an attempt to adapt to such a situation by utilizing individual FFT frequency cells as a bank of filters which can accommodate a broad variety of signals. The performance of the deflection detector is analyzed and compared to that of the

CONT

DD FORM 1 JAN 73 1473 EDITION OF 1 NOV 65 IS OBSOLETE

UNCLASSIFIED

SECURITY CLASSIFICATION OF THIS PAGE (When Data Entered)

20. Abstract (continued)

power detector for several seismic signals. It is concluded that the deflection detector shows a distinct advantage when the variety of signal spectra to be detected is sufficiently large.

ABSTRACT

ABSTRACT

This study investigates the application of a deflection detector to short-period seismic data. In general, for power detectors, no single filter will be optimal for a large variety of signals in a dynamic noise environment. The deflection detector represents an attempt to adapt to such a situation by utilizing individual FFT frequency cells as a bank of filters which can accommodate a broad variety of signals. The performance of the deflection detector is analyzed and compared to that of the power detector for several seismic signals. It is concluded that the deflection detector shows a distinct advantage when the variety of signal spectra to be detected is sufficiently large.

ACCESSION for		
NTIS	White Section	X
DDC	Buff Section	☐
UNANNOUNCED		☐
JUSTIFICATION		
BY		
DISTRIBUTION/AVAILABILITY CODES		
Dist.	AVAIL. and/or SPECIAL	
A		

Neither the Advanced Research Projects Agency nor the Air Force Technical Applications Center will be responsible for information contained herein which has been supplied by other organizations or contractors, and this document is subject to later revision as may be necessary. The views and conclusions presented are those of the authors and should not be interpreted as necessarily representing the official policies, either expressed or implied, of the Advanced Research Projects Agency, the Air Force Technical Applications Center, or the U.S. Government.

TABLE OF CONTENTS

LIST OF FIGURES

LIST OF FIGURES
(continued)

LIST OF TABLES

SECTION I
INTRODUCTION

The purpose of this study is to investigate the feasibility of applying a deflection detector to short-period seismic events recorded at the Korean Seismic Research Station (KSRS). Another goal is to design detector algorithms which operate on a variety of signal spectra with better operating characteristics than would be obtained by a power detector. For any detector, the ideal receiver will match its input time gate to the signal duration and its bandwidth to the signal and noise spectra. However, when a variety of (possibly unknown) signals are being detected in a dynamic noise environment, compromises are necessary. In general, no one filter will be optimal for a large class of signals. The deflection detector represents an attempt to adapt to such a situation by utilizing the individual frequency cells of an FFT (Fast Fourier Transform) as a bank of filters which can accommodate signals with widely differing spectra. At each time gate, the discrete spectral power is measured from the lowest frequency of interest to the highest frequency of interest. These spectral powers comprise the time series of spectral data from which detection statistics will be derived.

The details of the detector design are described in Section II. A statistical analysis of the detector's performance with seismic noise is given in Section III. Receiver Operating Characteristics (ROC) are presented in Section IV based on detector trials on four representative KSRS signals with seismic noise added to their waveforms. Conclusions and suggestions for further study are given in Section V.

SECTION II
THEORY

A. DEFLECTION DETECTOR

The deflection processor is a frequency domain detection technique. It detects large power deflections measured in individual FFT (Fast Fourier Transform) cells.

A moving time window of $2N$ points of seismic data is input to the detector and Fourier transformed. The power spectrum, or in some cases the log power spectrum, is found at N discrete points in the usual way. The power or log power at the k^{th} frequency, where k ranges from 1 to N, is normalized by subtracting its mean value and dividing the result by its standard deviation. Thus for the i^{th} segment of data we have

$$Z_i(k) = \frac{P_i(k) - \mu(k)}{\sigma(k)} \qquad \text{(II-1)}$$

where $P_i(k)$ is the power at the k^{th} frequency for the i^{th} time segment, $\mu(k)$ is the mean of the power at the k^{th} frequency, and $\sigma(k)$ is its standard deviation. Regarding k as fixed for the moment, we can think of $Z_i(k)$ as a random function of the variable i, with zero mean and unit standard deviation. There are a total of N such variables, one for each frequency index k.

At each value of i, i.e., for each input segment, we choose the largest value of the set $Z_i(k)$, where k is now varied to find the maximum over the frequency range of interest. It is legitimate to make this comparison over frequency, since each power has been normalized. If this

maximum exceeds some preset value, called the detection threshold, a detection is declared.

The parameters $\mu(k)$ and $\sigma(k)$ must be estimated from signal-free sections of data. Finding the best way to do this is one of the important problems of detector design, see Appendix A.

Another detector, called the average deflection power detector, is also evaluated here. It is denoted X_i at the i^{th} segment and is derived from the deflection detector through

$$X_i = \frac{1}{N} \sum_{\substack{\text{signal} \\ \text{band}}} Z_i(k). \qquad \text{(II-2)}$$

These detectors are compared to one operating in the time domain and described by Swindell and Snell (1977). There the data are prefiltered and the average power computed over a suitable time segment. This power is normalized by subtracting the mean power and dividing by the standard deviation, and the resulting quantity compared to a threshold. In the present study this form of detector was implemented in the frequency domain through the equations

$$Y_i = \frac{\left\{\frac{1}{N\Delta t} \sum_{\substack{\text{signal} \\ \text{band}}} P_i(k)\right\} - \mu}{\sigma} . \qquad \text{(II-3)}$$

Here Δt is the sampling period of the data, so by Parseval's theorem the bracketed quantity is the average power over the i^{th} data segment. The mean and standard deviation of the average power are μ and σ, respectively, which must be computed from signal-free data.

While the variables X_i, Y_i, and Z_i have unit standard deviation and zero mean, all other details of their distribution are unknown for the moment.

B. PROCESSING TECHNIQUES

1. Normalization

The comparison of different statistical distributions is basic to the concept of the deflection processor. As described in the previous subsection, its fundamental assumption is that the mean and standard deviation of the noise are sufficient to determine the detectability of the signal. Actually, this is strictly true only when the power distributions of the individual FFT cells, denoted ρ_N for noise alone and ρ_{S+N} for signal-plus-noise, possess the properties

(i) ρ_N is determined by its first two moments, μ and σ, where μ and σ may be independently specified.

(ii) $\rho_{S+N}(x) = \rho_N(x-c)$ where c is a constant; i.e., the presence of a signal merely translates the probability distribution a fixed distance, c.

An examination of the noise distributions for the seismic data under consideration (see Section III) revealed that the logarithm of the spectrum produced nearly normal distributions. For convenience in later calculations it was decided to perform a logarithmic transformation on the spectral power, P(k),

$$P'(k) = \log P(k) . \qquad \text{(II-4)}$$

Note that this implies that the mean $\mu'(k)$ and standard deviation $\sigma'(k)$ of the noise are computed after taking the logarithm of the spectrum:

$$\mu'(k) = E(\log P(k))$$

$$\sigma'(k)^2 = E\left[(\log P(k))^2 - \mu'(k)^2\right] . \qquad \text{(II-5)}$$

For purposes of comparison, the detector is also evaluated without logarithmic transformation.

2. Coherent Versus Incoherent Gain

Consider a particular signal spectrum $S(k)$ to be detected in noise having a mean spectrum $\mu(k)$ and a standard deviation $\sigma(k)$. The most probable frequency cell $\hat{k}$ for detection of the signal by the deflection processor is the one for which $Z(k)$ is a maximum. In practice, it was found that this condition was satisfied in most cases by a single frequency cell of the 32-point FFT transform (see Section IV). Thus, the deflection detector is approximately equivalent to that pictured in Figure II-1(a). Similar diagrams are given for the deflection-power detection and the conventional power detector in Figures II-1(b) and II-1(c).

An examination of Figure II-1 reveals that the deflection processor provides two types of gain. The first, commonly referred to as coherent gain (CG), is the result of maximizing $Z_i(k)$ and is given (in decibels) by

$$CG_d = 10 \log_{10} \frac{(\text{signal/noise})_{\text{cell } \hat{k}}}{(\text{signal/noise})_{\text{signal band}}}$$

$$= 10 \log_{10} \frac{S(\hat{k}) / \mu(\hat{k})}{\sum_{\substack{\text{signal} \\ \text{band}}} S(k) \Big/ \sum_{\substack{\text{signal} \\ \text{band}}} \mu(k)} \quad . \qquad \text{(II-6)}$$

(Note that for some spectra this may be less than zero dB; i.e., a loss.) The second gain, so-called incoherent gain, is the reduction of noise standard deviation obtained when the maximum of a set of N random variables is itself treated as a random variable. In the present case, the logarithms of the normalized noise powers in the i^{th} data segment have an (approximately) Gaussian distribution, but the distribution of their maxima $Z(\hat{k})$ is given by

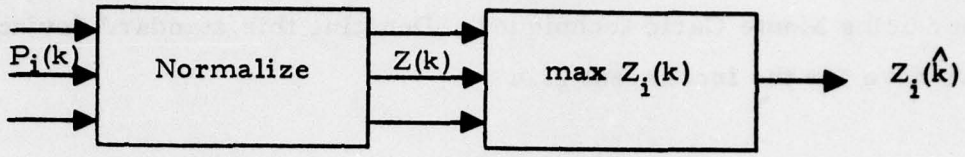

(a) Deflection

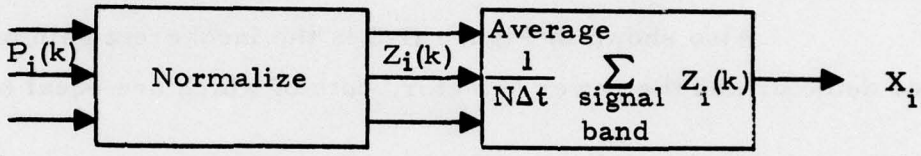

(b) Deflection-Power

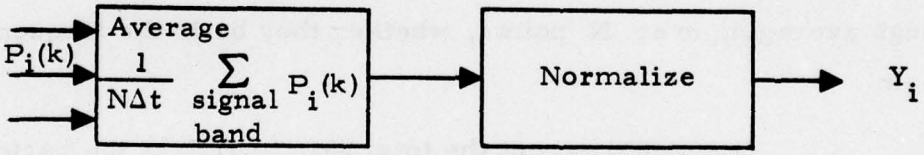

(c) Power

FIGURE II-1

ABBREVIATED MODELS OF THREE DETECTORS

$$P(Z(\hat{k})) = \left\{ \int_{-\infty}^{Z(\hat{k})} G(x)dx \right\}^{N-1} \cdot G(Z(\hat{k})) \qquad \text{(II-7)}$$

where $G(x)$ is the Gaussian probability density. The standard deviation of G is difficult to find analytically, but may be obtained in a straightforward manner using Monte Carlo techniques. Denoting this standard deviation by σ_Z, we have for the incoherent gain

$$IG_d = 10 \log (1/\sigma_Z) . \qquad \text{(II-8)}$$

This quantity is plotted as a function of N in Figure II-2.

Also shown in Figure II-2 is the incoherent gain of the deflection-power detector and the power detector, both of which are equal to

$$IG_p = 10 \log \sqrt{N} . \qquad \text{(II-9)}$$

This gain is due to reduction of the standard deviation of the noise power through averaging over N points, whether they be in the frequency or time domain.

One would expect the total gain to reflect the performance of the detectors. Strictly speaking, this is true only in the case where $\rho_{S+N}(x) = \rho_N(x-c)$. Furthermore, the incoherent gains for the deflection detector and deflection-power detector are those indicated only when the distributions of the individual frequency cells are identical (e.g., flat signal and flat noise spectrum) and Gaussian. Thus, in general, equations (II-5) and (II-6) provide only a guideline to the relative effectiveness of the three detectors. The degree of reliance that one may place on these indicators will be treated in Section IV.

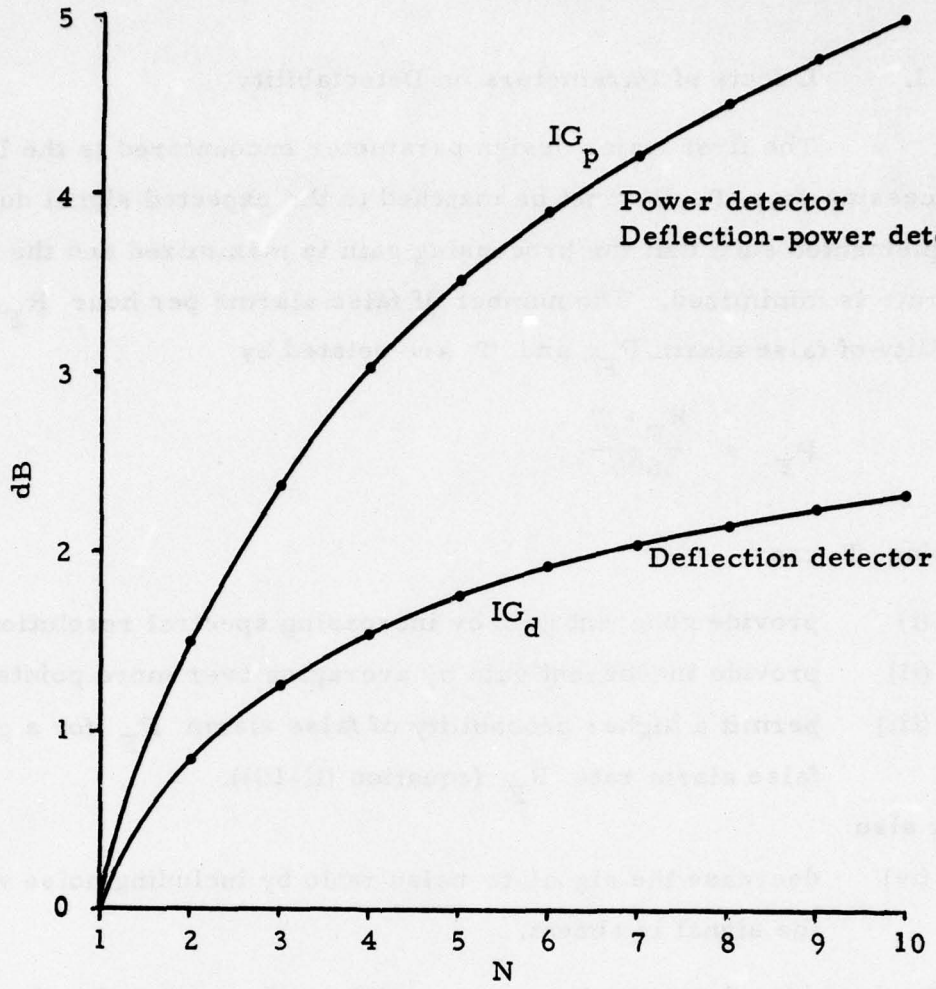

FIGURE II-2

INCOHERENT GAINS VERSUS NUMBER OF FREQUENCY CELLS FOR THE POWER, DEFLECTION-POWER, AND DEFLECTION DETECTORS

3. Effects of Parameters on Detectability

The first major design parameter encountered is the length of the processing gate T. It must be matched to the expected signal duration and implemented such that the processing gain is maximized and the false alarm rate is minimized. The number of false alarms per hour R_F, the probability of false alarm P_F, and T are related by

$$P_F = \frac{R_F \cdot T}{3600} . \qquad \text{(II-10)}$$

Increasing T can

(i) provide coherent gain by increasing spectral resolution,

(ii) provide incoherent gain by averaging over more points, and

(iii) permit a higher probability of false alarm P_F for a given false alarm rate R_F (equation (II-10)),

but may also

(iv) decrease the signal-to-noise ratio by including noise where the signal is absent.

Thus, T should be chosen as large as possible without incurring the penalty (iv).

Assuming that an appropriate T has been chosen for the variety of signals to be detected, a subdivision into FFT gates may be made. It is advisable to overlap processing gates in order to match the signal start time as closely as possible. Increasing the number of overlapping segments M trades off a possible coherent gain (i.e., decreases FFT resolution) for an incoherent gain coupled with a better chance of matching the start of the signal. Overlap may also be obtained without increasing M, but at the expense of performing more FFT transforms. There is no change in P_F because, although the number of outputs are increased, they are statistically

dependent, and the inclusion of an M-output-gate dead time after a detection prevents a doubling of the alarm rate.

Another parameter of importance is the prefilter. For a given variety of signals and noise spectra it is obviously advantageous to filter out those portions of the spectrum which consist primarily of noise. An extreme example is presented when the signal to be detected and the noise statistics are completely known. In that case, for a given P_F, there exists a filter which will optimize the probability of detection P_D for the power detector. Since, for a single signal, the deflection detector is approximately a power detector with a narrowband prefilter, it would in general perform more poorly than such an optimum filter (i. e., the narrowband filter would not be optimal). If, however, the variety of signals to be detected is large, a single optimum filter is not possible since one does not wish to filter one signal at the expense of another, and a likely choice for the prefilter is a simple bandpass filter. It should be noted that a specific advantage of the deflection processor is that it provides a bank of filters (the FFT cells) as opposed to a single filter which may be utilized in detecting a broad variety of signals.

Finally, let us consider the size of the time constant used in updating estimates of the noise statistics. If, as in the present study, the background noise is only quasi-stationary, the noise statistics must be periodically updated. When such an update involves a time average, the averaging time should be chosen short enough to insure short-term stationarity and yet long enough to provide a reliable estimate. This is extremely important because the results will directly affect the choice of a detection threshold. While a detector's ROC curves (P_F versus P_D) are independent of any choice of threshold, the actual performance of the detector is not. If a threshold (possibly time dependent) cannot be set to provide a desired false alarm rate, then even a superior detector may be impractical to implement or may perform poorly.

SECTION III
NOISE STATISTICS

The design of a detector requires an accurate signal model and knowledge of the statistical properties of the noise in which it is embedded. Thus, it is imperative to examine the noise statistics as extensively as possible. To do this one must choose a homogeneous ensemble of independent noise samples. If the noise is not stationary (but only one sample is available at a given time), the ensemble must be chosen within a short enough time period to insure approximate stationarity.

In the present case, a continuous 2 hour 40 minute sample of noise was edited from a Korean Seismic Research Station (KSRS) data tape for examination and beamformed at 20 km/sec. The 96,000 points (obtained at a sample rate of 10/sec) were divided into 3,000 gates of 3.2 seconds each corresponding to a 32-point FFT, and into 6,000 gates of 1.6 seconds, corresponding to a 16-point FFT. The gates were Fourier transformed and the statistics of the noise power $N(k)$ for each frequency cell k were studied. Tests indicated independence of the samples N_i, $i = 1, \ldots, 3000$ with 95% confidence. The original noise samples, 0.1 second apart, were not independent (i.e., their spectrum was not flat). In addition, application of the Kolmogorov-Smirnov two-sample test indicated homogeneity with 95% confidence.

The mean and standard deviation of the power spectrum and of the total power are plotted in decibels versus frequency in Figure III-1.

It is well known that the power of seismic noise is approximately log-normal (Freedman, 1967; Swindell and Snell, 1977). This

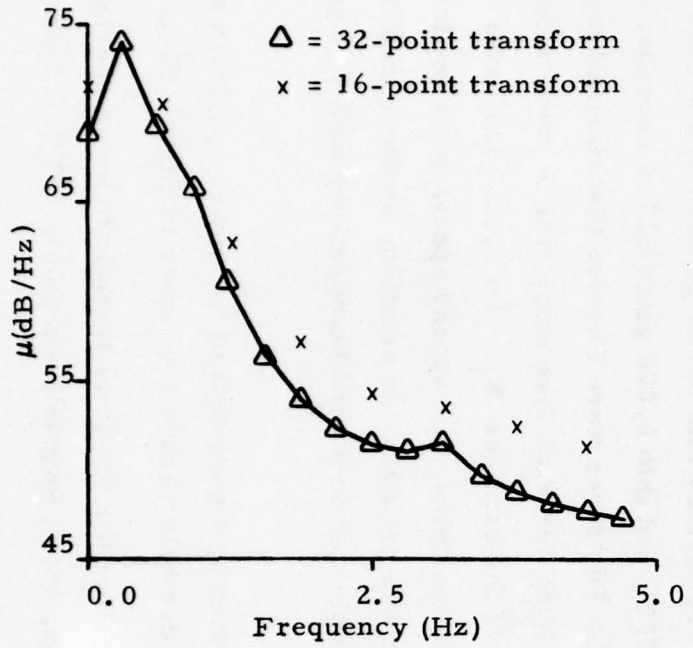

(a)

μ_T = 59.5 dB

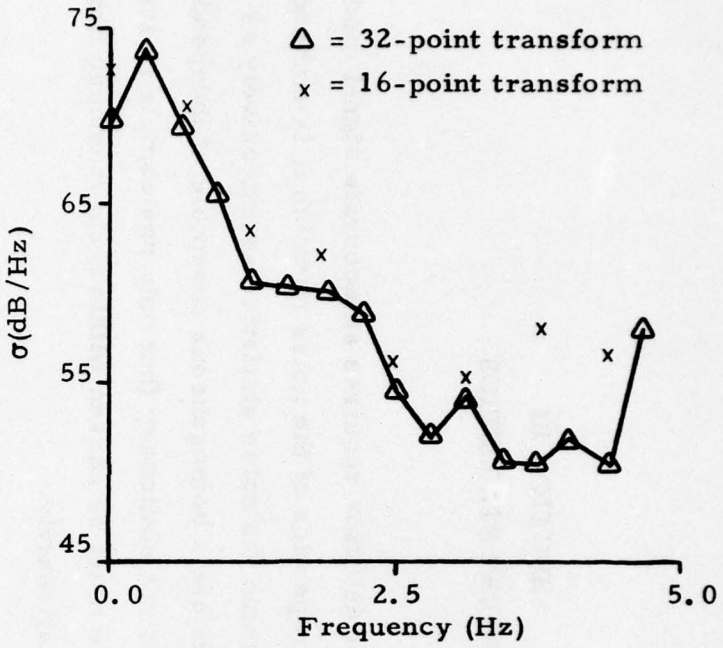

(b)

σ_T = 57.2 dB

FIGURE III-1

PLOTS OF THE (a) NOISE POWER SPECTRUM $\mu(k)$ AND (b) NOISE POWER STANDARD DEVIATION $\sigma(k)$. ALSO INDICATED ARE THE MEAN OF THE TOTAL POWER, μ_T AND ITS STANDARD DEVIATION, σ_T FOR A 3.2 SEC. GATE

leads us to the conjecture that the same may be true of narrowband seismic noise (at resolutions of 0.3 Hz and 0.6 Hz). To test this hypothesis, the logarithms of the noise spectrum samples were taken and the resulting ensembles examined. The means and standard deviations of these distributions appear in Figure III-2.

Goodness-of-fit tests were made to test the normality of the log power distributions; the results appear in Table III-1. Although the distributions of individual FFT cells are different, those above 1.0 Hz all appeared approximately normal at the 0.05 critical level corresponding to the test value. Note that no single cell was as close to normal as the logarithm of the total power (i.e., broadband noise). Examples of some of the individual distributions are found in Figures III-3 and III-4.

The above noise sample would appear sufficiently long to set a threshold for false alarm rates on the order of two per hour (i.e., that value which the detector output exceeds only six times in the entire 2 2/3 hour noise sequence). However, such low alarm rates depend only on the tail of the distribution and as a result are inordinately sensitive to relatively small fluctuations in the statistics. In other words, short-term noise variations will have a noticeable effect on the threshold. This poses the following dilemma: A long time period is necessary to estimate the threshold, but the threshold must be dynamic over a much shorter period.

One possible solution (that adapted here) is to assume that the noise distributions in question depend to a 'close' approximation only on their first two moments. These parameters, the mean and standard deviation, may be estimated from a much smaller ensemble than would be required for the accurate determination of the tail of the distribution. Once the mean and standard deviation have been found, a normalization transforms the distribution to a canonical one, reasonably independent of the statistical fluctuations, and the appropriate threshold may be set.

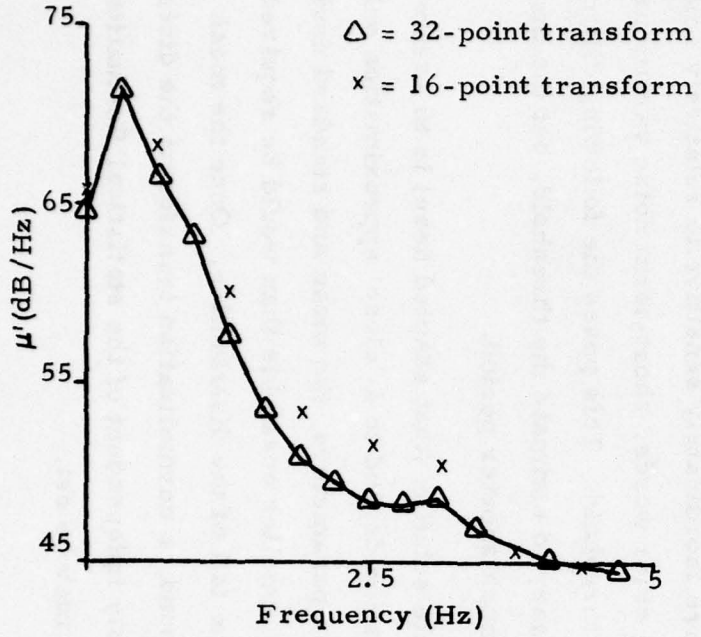

(a)

μ'_T = 58.8 dB

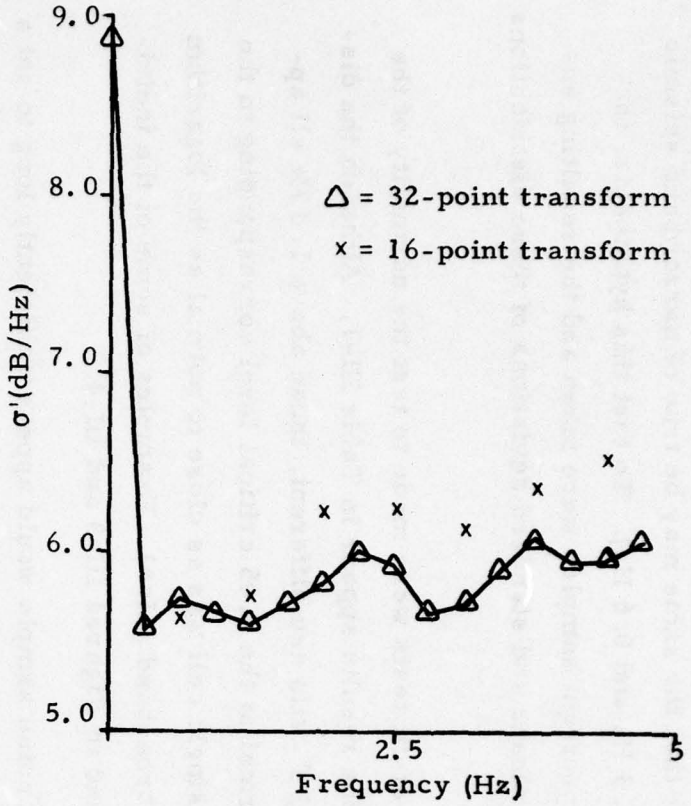

(b)

σ'_T = 2.4 dB

FIGURE III-2

PLOTS OF (a) THE AVERAGE OF THE LOGARITHM OF THE NOISE POWER $\mu'(k)$ AND (b) ITS STANDARD DEVIATION $\sigma'(k)$. ALSO INDICATED ARE THE MEAN OF THE LOGARITHM OF THE TOTAL POWER, μ'_T AND ITS STANDARD DEVIATION, σ'_T FOR A 3.2 SECOND GATE

TABLE III-1

RESULTS FOR TESTS FOR NORMALITY OF 500-POINT ENSEMBLES FOR FREQUENCY CELLS 2, 4, AND 6 AND TOTAL POWER IN A 1.6-SECOND GATE; AND CELLS 4, 8, AND 12 AND TOTAL POWER IN A 3.2-SECOND GATE

	(0.6 Hz Resolution) 16-Point Transform				(0.3 Hz Resolution) 32-Point Transform				
Frequency Cell	2 (0.65 Hz)	4 (1.9 Hz)	6 (3.1 Hz)	Total Power	4 (0.9 Hz)	8 (2.2 Hz)	12 (3.4 Hz)	Total Power	Test Value
Chi-square goodness-of-fit test statistic	108	62	67	59	109	58	68	52	57
Kolmogorov-Smirnov test statistic	0.101	0.056	0.048	0.040	0.084	0.048	0.062	0.048	0.061

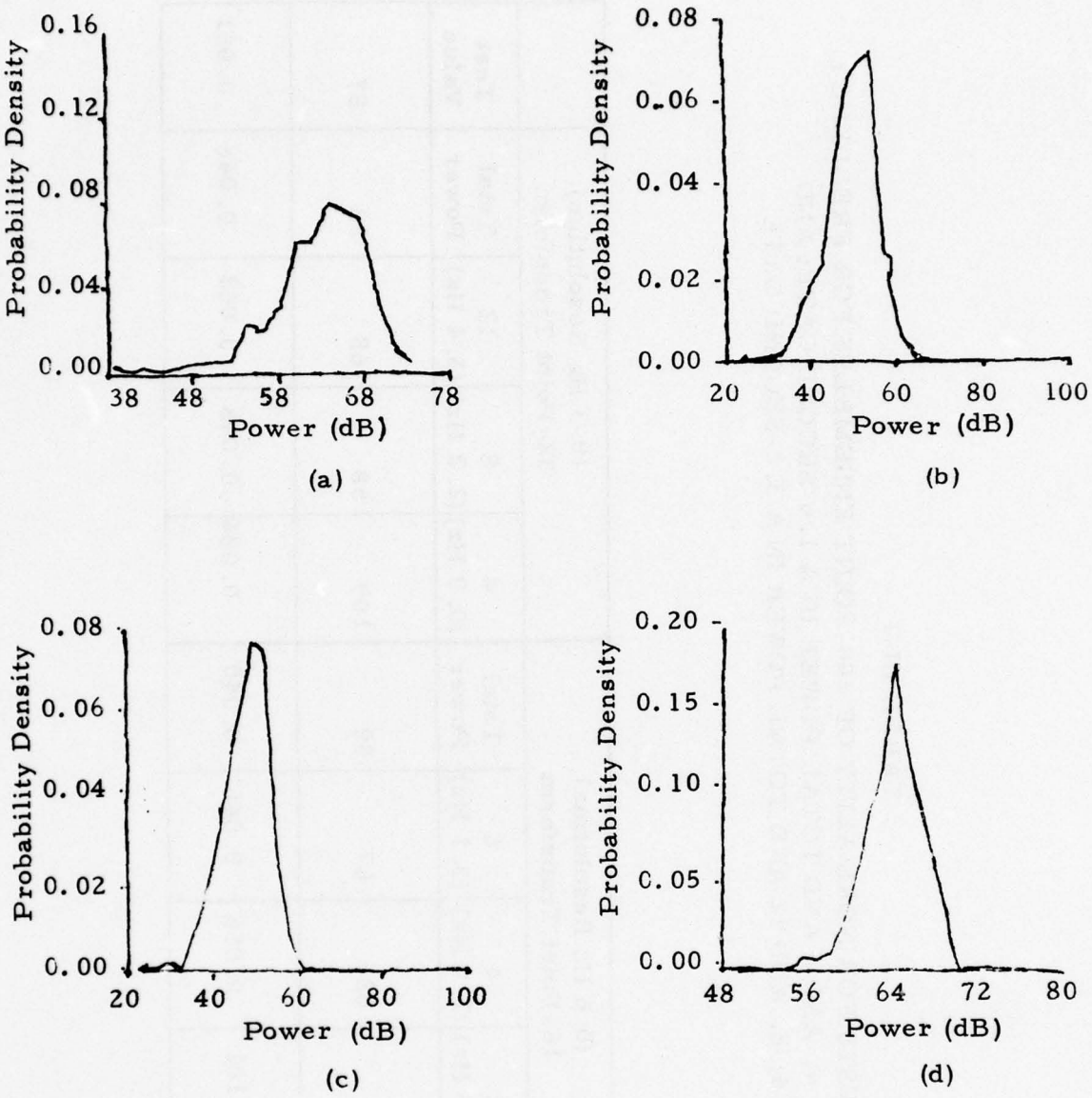

FIGURE III-3

EMPIRICAL DISTRIBUTIONS FOR 500-POINT ENSEMBLES FOR (a) 0.9 Hz (CELL 4) (b) 2.2 Hz (CELL 8) (c) 3.5 Hz (CELL 12) AND (d) TOTAL POWER FOR A 32-POINT TRANSFORM

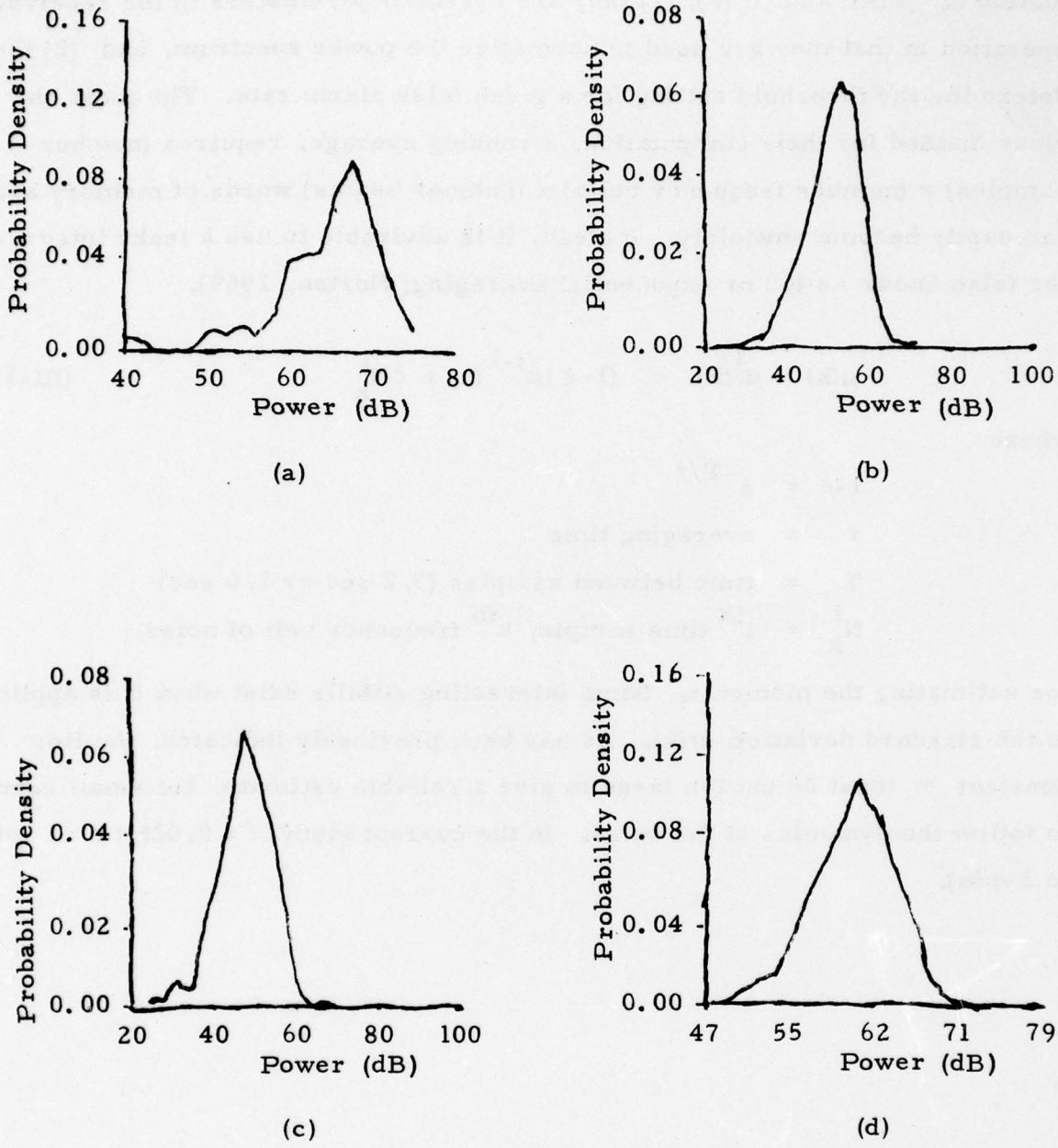

FIGURE III-4

EMPIRICAL DISTRIBUTIONS FOR 500-POINT ENSEMBLES FOR (a) 0.6 Hz (CELL 2) (b) 2.0 Hz (CELL 4) (c) 3.2 Hz (CELL 6) AND (d) TOTAL POWER FOR A 16-POINT TRANSFORM

We now have two compelling reasons for accurate on-line estimation of $\mu'(k)$ and $\sigma'(k)$; (1) they are essential parameters in the receiver's operation in that they are used to normalize the power spectrum, and (2) they determine the threshold setting for a given false alarm rate. The most obvious method for their computation, a running average, requires (number samples) x (number frequency cells) x (number beams) words of memory and can easily become unwieldly. Instead, it is advisable to use a leaky integrator (also known as RC or exponential averaging; Horton, 1969),

$$\mu(k) \sim \mu^{i}(k) = (1-\epsilon)\mu^{i-1}(k) + \epsilon N_k^i \qquad \text{(III-1)}$$

where

$1-\epsilon = e^{-T/\tau}$

τ = averaging time

T = time between samples (3.2 sec or 1.6 sec)

N_k^i = i^{th} time sample, k^{th} frequency cell of [illegible]e,

for estimating the moments. Some interesting pitfalls exist when it is applied to the standard deviation $\sigma(k)$. As has been previously indicated, the time constant τ must be chosen large to give a reliable estimate, but small enough to follow the dynamics of the noise. In the current study $\epsilon = 0.025$ (τ = 1 min to 2 min).

SECTION IV
EVALUATION

A. INTRODUCTION

The evaluation of a detector is not often an easy task. For the simple case of a known signal in Gaussian noise, the detectability depends only on the ratio of the signal power to the standard deviation of the noise which in turn is proportional to the signal-to-noise ratio (Van Trees, 1968). The greater this value, the greater the probability of detection (P_D) for a given probability of false alarm (P_F). For more complex situations, a rough estimate of detectability is the 'deflection' criterion:

$$\frac{E\left[f(s+n) - f(n)\right]}{\sigma(f(n))} \qquad \text{(IV-1)}$$

where

$f(x)$ = detector output for input x

s = signal

n = noise

$\sigma(x)$ = standard deviation of x

which gives the 'distance' between the output distributions for signal-plus-noise and for noise alone. By varying the signal standard deviation, one can construct two detector outputs x and y such that x detects more signals than y but y gives a larger deflection criterion for all P_F. It is also possible for one detector to be better at low false alarm rates while another is better when they are high. In short, for most detectors it is necessary to actually compute their ROC curves (graphs of P_D versus P_F) in order to evaluate their performance.

These curves depend on the detector, the signal being detected, and the noise statistics. In general, for a fixed signal, an increase in signal power should provide higher detectability; i.e., all points on the ROC curve would move upwards. To determine ROC curves by compiling a large number of seismic events is impossible since no two signals will have the same shape, and estimates of their magnitude are approximate. Thus, the following procedure was implemented.

A seismic event $s(t)$ of duration T seconds was chosen, beamformed and edited. Several thousand noise samples $n_i(t)$ of the same duration, T, were also edited. The detector was then run separately on the samples $n_i(t)$ (noise alone) and $\alpha s(t)+n_i(t)$ (signal-plus-noise at a fixed peak signal-to-RMS-noise ratio dependent on α). For each value of α, a ROC curve was computed from the two output distributions (see Figure IV-1 for details).

In the present study, the processing gate T was taken to be 3.2 seconds, while FFT transforms of both 16 and 32 points were examined. In the former case the probability distributions were determined from 6000 sample points; in the latter, from 3000. Six ROC curves were computed for values of α corresponding to signal-to-noise ratios of -6 dB, -3 dB, 0 dB, 3 dB, 6 dB, and 9 dB. For each curve the probability of detection, P_D, was plotted for false alarm probabilities of P_F= 0.001, 0.002, 0.004, 0.008, 0.02, and 0.04, corresponding to false alarms of 1.1, 2.2, 4.5, 9.0, 22.5, and 45.0 per hour. This was sufficient for comparing detectors even though some lower rates, less than P_F= 0.001, would also be of interest. We note that for P_F= 0.001 and only 3000 sample points, the results are subject to some statistical variation, and for even smaller values a larger sample space would certainly be necessary.

Four representative short-period seismic events recorded at KSRS were beamformed and edited (32 sample points at a rate of 10 per

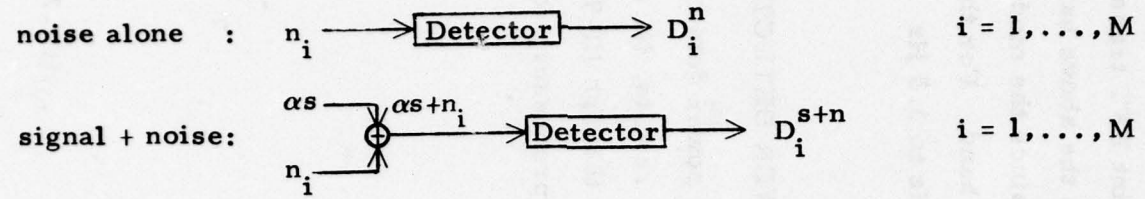

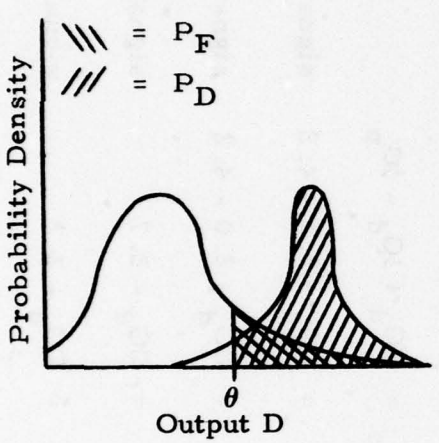

$$P_F = \frac{\text{number } D_i^n > \theta}{M}$$

$$P_D = \frac{\text{number } D_i^{s+n} > \theta}{M}$$

θ = detection threshold

FIGURE IV-1

CONSTRUCTION OF A ROC CURVE (COORDINATES ($P_F(\theta)$, $P_D(\theta)$)) USING AN M-POINT SAMPLE SPACE

second) for use as signals in evaluating the detector. These signals, referred to as A, B, C, and D, are documented in Table IV-1, and their spectra appear in Figure IV-2. Note the presence of high frequency energy in C and D (presumed explosions) not found in A and B. The three hours of noise analyzed in Section III was also used in the simulation. The prefilter consisted of a bandpass filter from 0.8 Hz to 3.6 Hz (cells 4 to 12 in a 32-point FFT transform). However, for event C, the low signal-to-noise ratio in the above band (2.3 dB) necessitated a narrower prefilter (1.4 Hz to 3.6 Hz) since the model signal could not be accurately estimated throughout the larger band. For the 16-point transforms, the corresponding prefilters were 0.93 Hz to 3.5 Hz (cells 2 to 6) and 1.7 Hz to 3.5 Hz (cells 3 to 6).

B. COMPARISON OF DEFLECTION DETECTOR AND POWER DETECTOR

We now consider the performance of the two log power detectors described by equations (II-1) and (II-2). Before presenting the results, let us estimate the detectors' relative behavior using equations (II-6) through (II-9) and Figure II-2. For a 3.2-sec gate the gain of the deflection processor, for models A, B, C, and D documented in Table IV-1, is:

$$
\begin{aligned}
G_d - G_p &= CG_d + IG_d - IG_p \\
&= CG_d + 2.1 - 4.8 \quad \text{signals A, B, D} \\
&= CG_d + 2.0 - 4.2 \quad \text{signal C} \\
&= CG_d - 2.7 \quad \text{signals A, B, D} \\
&= CG_d - 2.2 \quad \text{signal C.}
\end{aligned}
\qquad \text{(IV-2)}
$$

Table IV-2 contains the calculation of the coherent gain and the numerical results.

TABLE IV-1

PARAMETERS OF NOISE AND FOUR SEISMIC SIGNALS RECORDED AT KSRS

Event	Lat.	Long.	Date	Origin Time	m_b	PDE Depth (km)	Azimuth (°)	Δ (°)
A	45.00	151.00	02/03/76	14.32.02	5.1	33	19.0	19.0
B	54.50	162.00	02/03/76	23.57.55	5.9	33	43.0	28.0
C	49.87	78.25	01/15/76	04.46.58	5.2	0	45.0	40.0
D	70.80	54.10	11/02/74	04.59.57	6.7	0	335.5	49.7
Noise	--	--	02/06/76	21.00.00 to 23.40.00	--	--	50.0	20.0

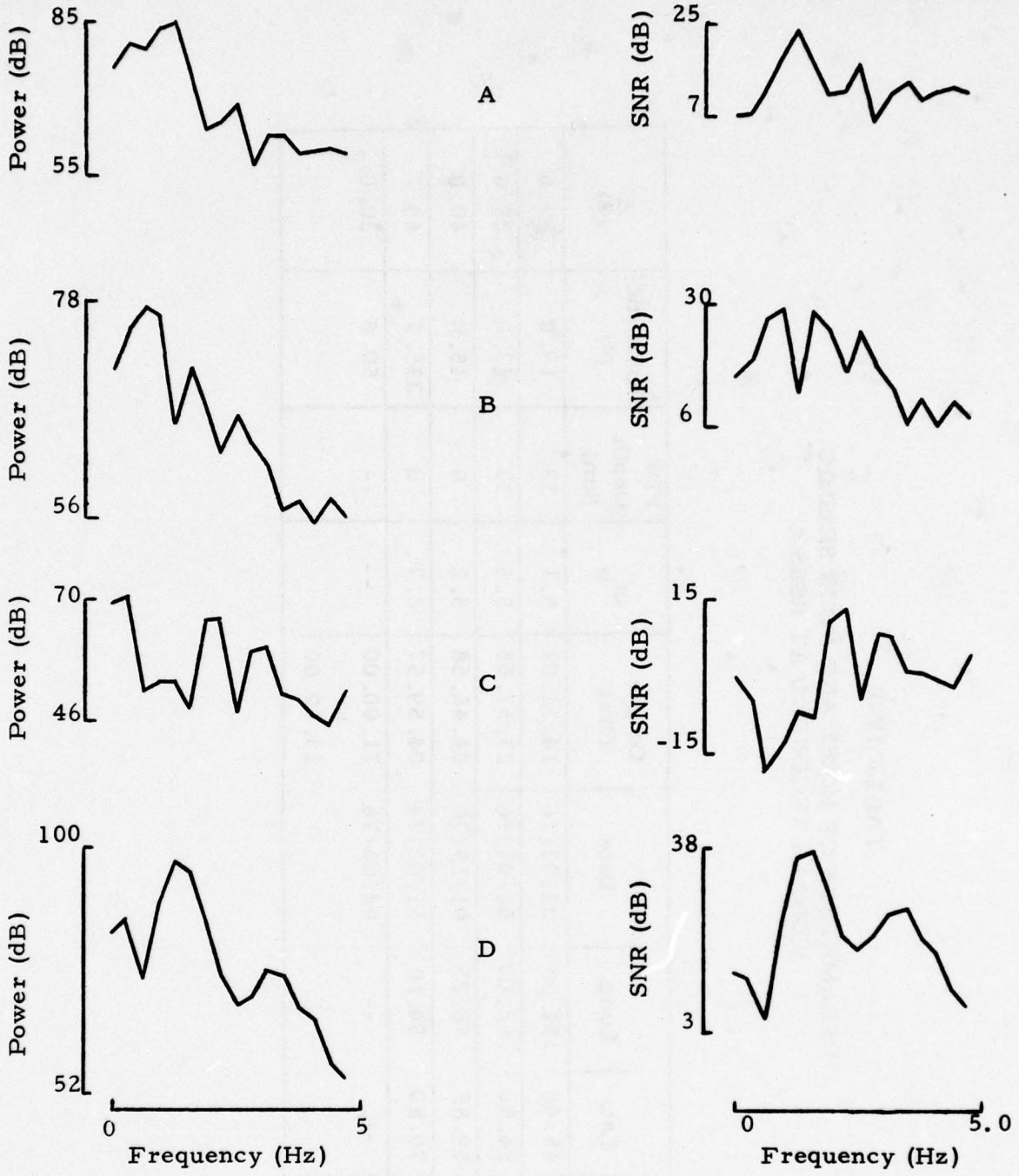

FIGURE IV-2

SPECTRA OF FOUR SIGNALS AND THEIR
SIGNAL-TO-NOISE RATIOS

TABLE IV-2

ESTIMATED GAIN OF DEFLECTION DETECTOR OVER
POWER DETECTOR FOR SIGNALS A, B, C AND D, (3.2 SEC. GATE)

Signal	Freq. Cell $\hat{k}$	Peak Sig Power in dB/Hz $S(\hat{k})$	Noise Power in dB/Hz at $\hat{k}$ $\mu(\hat{k})$	Total Sig Power (in dB) for Detection Band P_T	Total Noise Power (in dB) for Detection Band μ_T	Estimated Coherent Gain (dB) CG_d from equation (II-6)	Estimated Total Gain (dB) from equation (IV-2) $G_d - G_p$
A	5	84.9	60.4	83.0	62.8	4.3	1.6
B	4	95.2	65.6	90.8	62.8	1.6	-1.1
C	8	66.2	52.7	64.7	56.4	5.2	3.0
D	6	94.3	56.5	94.3	62.8	6.3	3.6

$$P_T = \frac{1}{3.2}\sum_{k=4}^{12} P(k) \quad \left.\right\} \text{A, B, D}$$

$$= \frac{1}{3.2}\sum_{k=6}^{12} P(k) \quad \left.\right\} \text{C}$$

$$\mu_T = \frac{1}{3.2}\sum_{k=4}^{12} \mu(k) \quad \left.\right\} \text{A, B, D}$$

$$= \frac{1}{3.2}\sum_{k=6}^{12} \mu(k) \quad \left.\right\} \text{C}$$

ROC curves for the four signals at signal-to-noise ratios of -6 dB, -3 dB, 0 dB, 3 dB, 6 dB, and 9 dB are pictured in Figure IV-3. It can be seen that in comparison with the power detector the deflection detector performs better for cases C and D, approximately equally for case A, and more poorly in case B. In order to estimate the actual gains and compare them with those predicted in Table IV-2, Figure IV-4 contains plots of P_D versus signal-to-noise ratio with P_F fixed at 0.004. As seen in Table IV-3, the actual gains found from Figure IV-4 reflect those estimated reasonably well, especially considering the approximate nature of our reasoning (i.e., the true gains depend in a non-linear manner on P_D, P_F, and even S/N). Loosely speaking, when the signal is concentrated at low frequencies, the region of highest noise, filtering provides little coherent gain and the power detector is preferable. For those having more high frequency energy (C and D), the deflection detector is better. (For the curious reader, a typical set of probability distributions (noise and signal-plus-noise) for S/N = 0 dB are included in Figure IV-5.)

C. VARIATIONS

Detection curves (at $P_F = 0.004$) comparing the effects on the deflection detector of the FFT transform length, the intermediate logarithmic transformation, and forming the deflection-power are found in Figures IV-6 and IV-7. A brief analysis of these results now follows.

1. 16-Point Transform

Let us examine the consequences of reducing the FFT transform length of the deflection detector from 32 to 16. According to Section II-B-3, this should exchange coherent gain for incoherent gain ($10 \log \sqrt{2} = 1.5$ dB). In Table IV-4, we estimate the performance of the detector relative to a 32-point transform and compare it with that deduced from Figure IV-6 by subtracting S/N for the 32-point transform from that for the 16-point

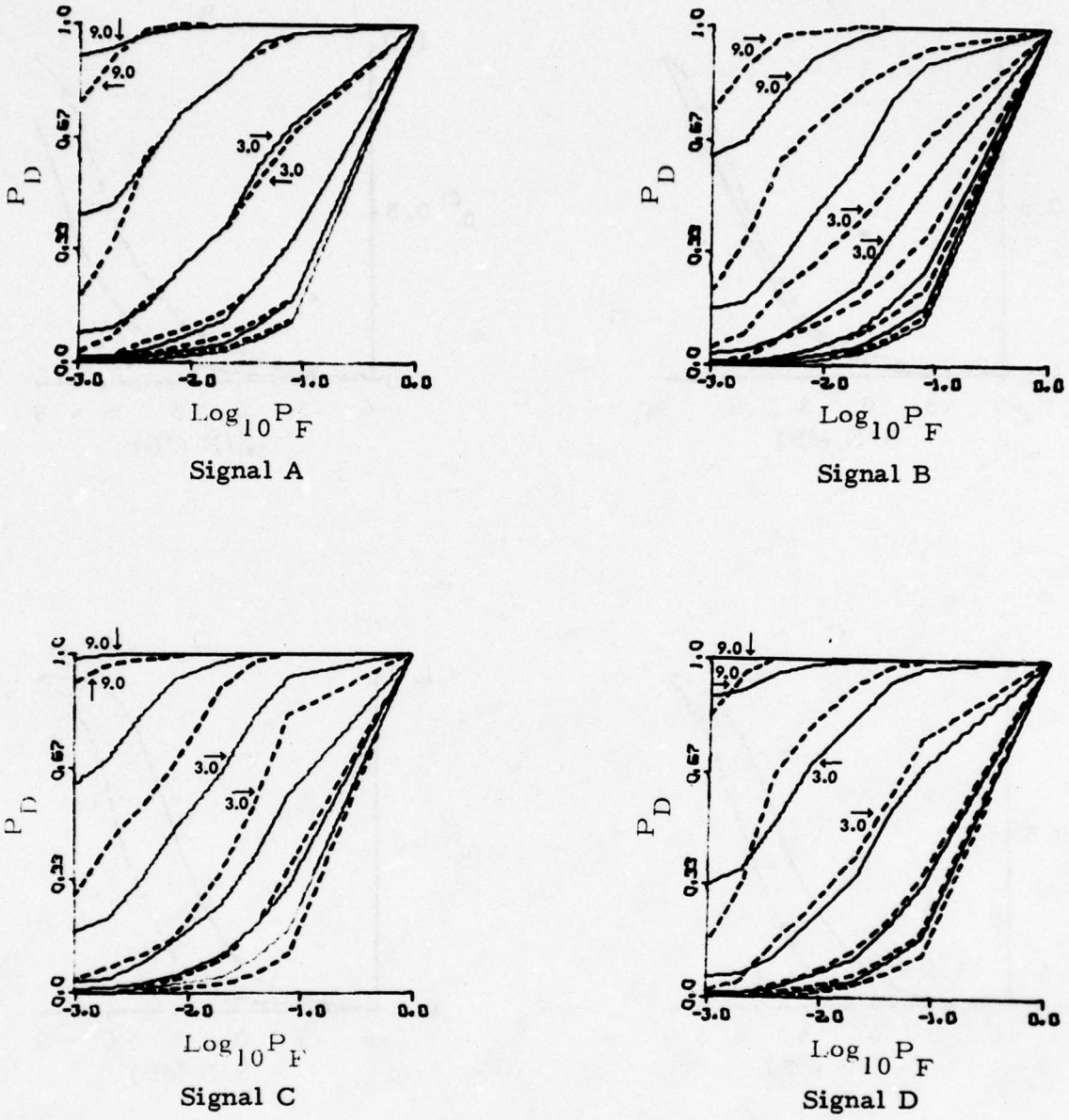

FIGURE IV-3

ROC CURVES (P_D VERSUS $LOG_{10}P_F$) FOR THE FOUR EVENTS A, B, C, AND D. FOR EACH EVENT THE ROC CURVES CORRESPOND TO SIGNAL-TO-NOISE RATIOS OF -1 dB, -3 dB, 0 dB, 3 dB, 6 dB, AND 9 dB. THE SOLID LINES BELONG TO THE DEFLECTION DETECTOR WHILE THE DASHED LINES ARE THOSE OF THE POWER DETECTOR

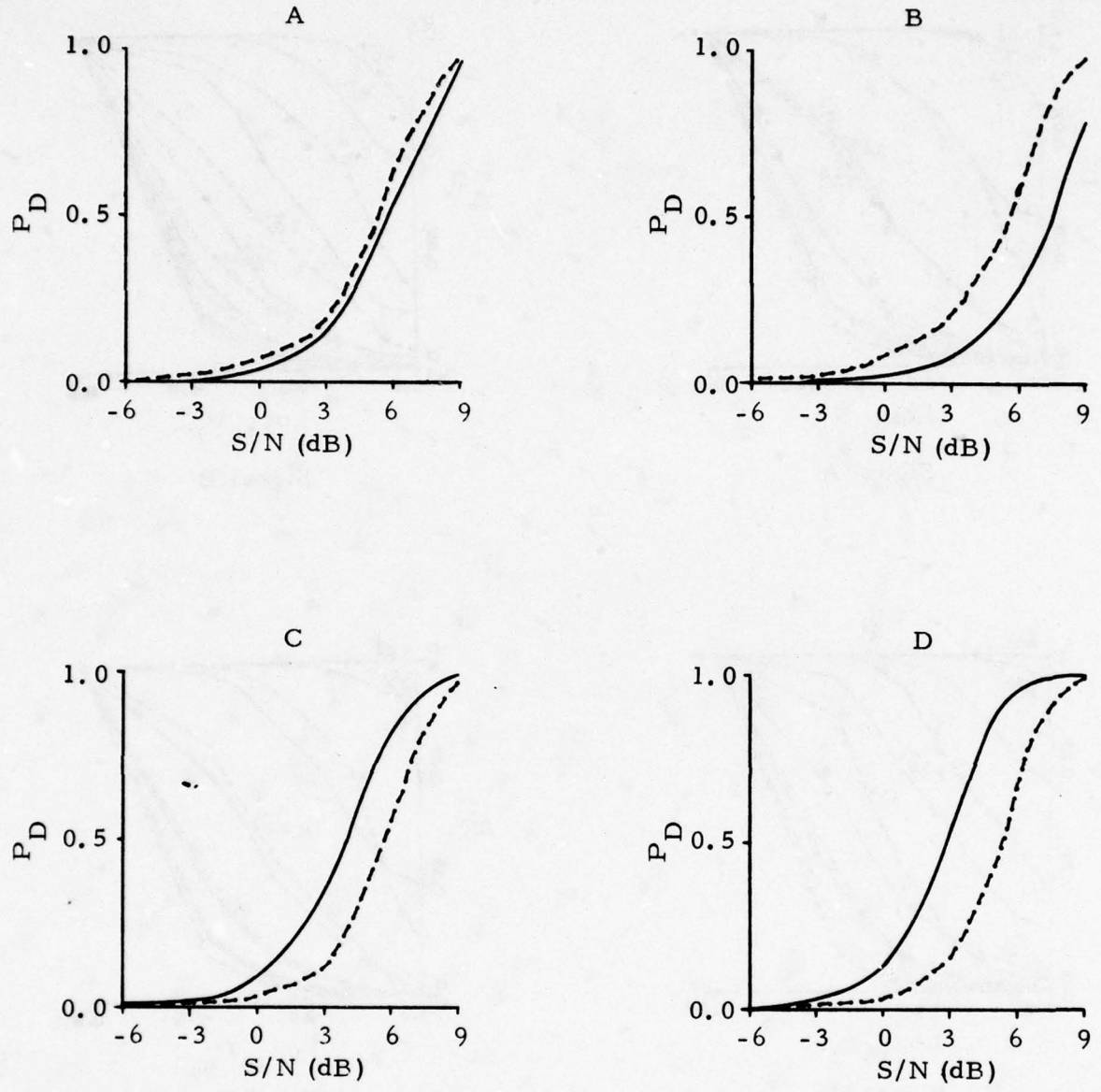

FIGURE IV-4

COMPARISON OF THE PERFORMANCE OF THE DEFLECTION DETECTOR (SCLID LINE) AND POWER DETECTOR (DASHED LINE) FOR A FALSE ALARM PROBABILITY OF P_F=0.004 (4.5 PER HOUR)

TABLE IV-3

COMPARISON OF ACTUAL GAINS
OF THE DEFLECTION DETECTOR OVER THE POWER DETECTOR
TO THOSE ESTIMATED (G_d-G_p) FOR FOUR SIGNALS

Signal	Estimated Total Gain	Actual Gain For $P_F = 0.004$; $P_D = 0.5$
A	1.6	-0.4 dB
B	-1.1	-1.9 dB
C	3.0	1.7 dB
D	3.5	2.5 dB

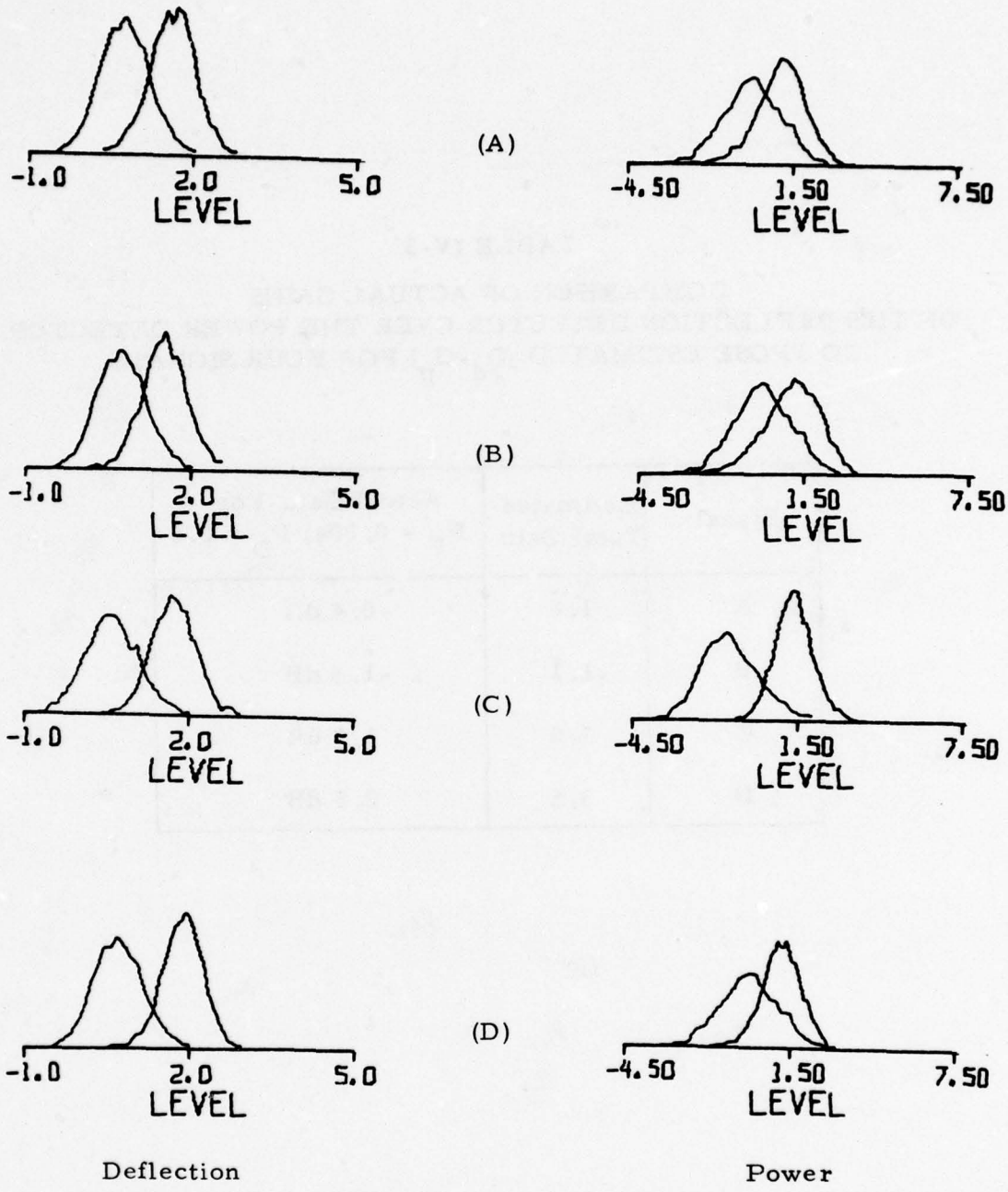

FIGURE IV-5

CUTPUT PRCBABILITY DISTRIBUTICNS FCR INPUTS CF NOISE AND OF SIGNAL-PLUS-NCISE (AT S/N = 0 dB) FCR DEFLECTION AND PCWER DETECTCRS; SIGNALS A, B, C, AND D

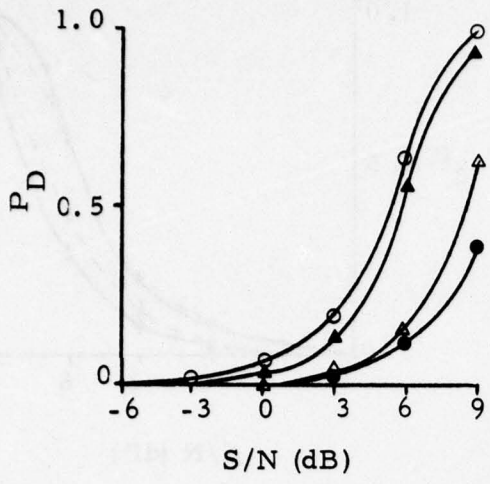

(A)

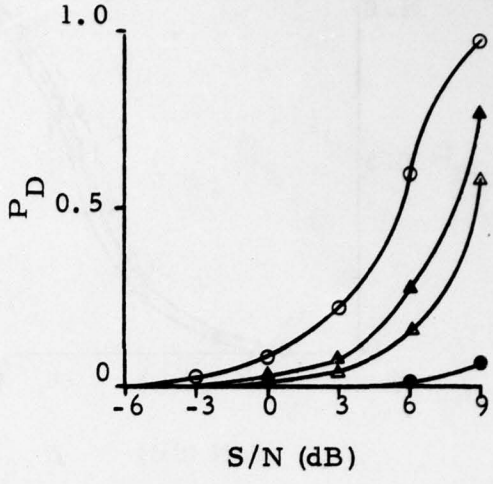

(B)

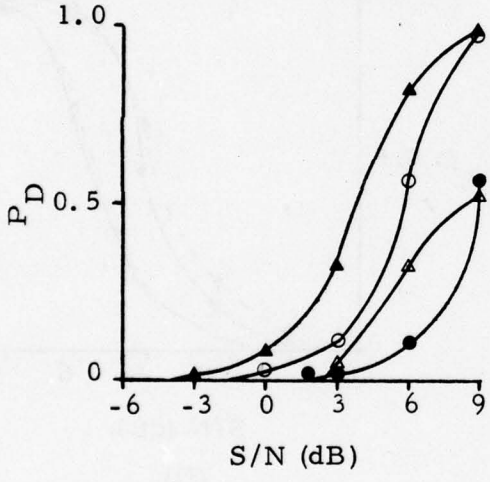

(C)

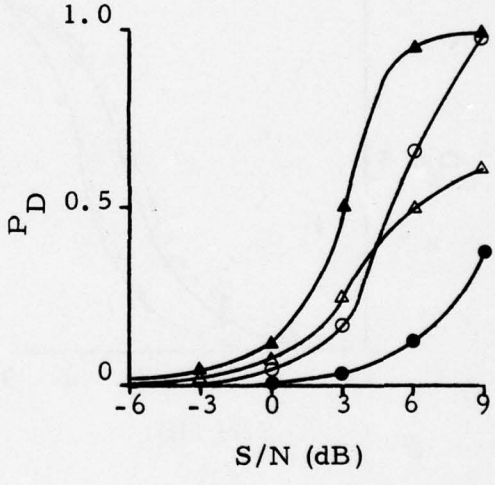

(D)

▲ = deflection detector 32 pt. transform
○ = power detector
● = deflection-power detector
△ = deflection detector 16 pt. transform

FIGURE IV-6

COMPARISON OF FOUR DETECTORS
FOR $P_F = 0.004$

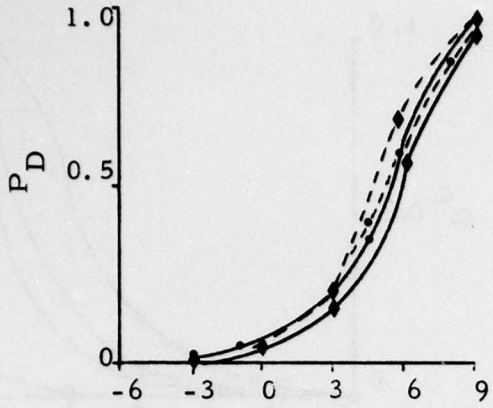

(A)

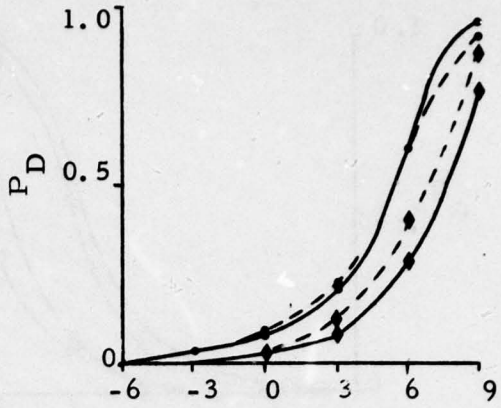

(B)

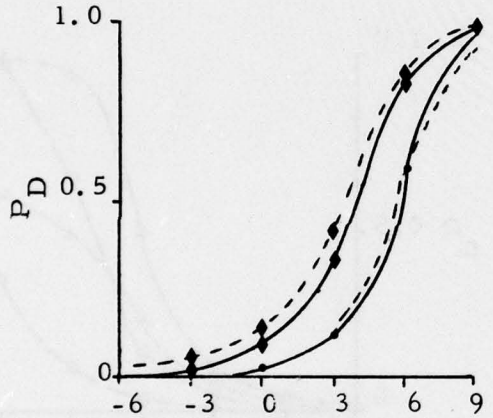

(C)

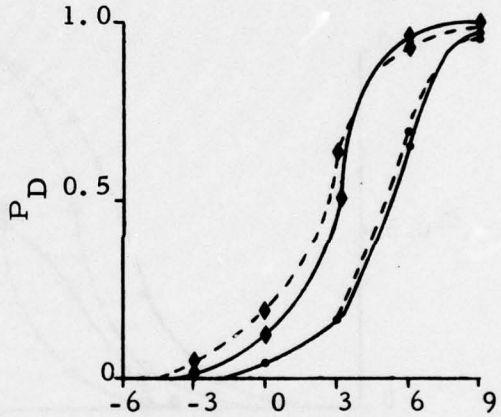

(D)

♦——♦ = deflection with logarithm
•——• = power with logarithm
♦- - - -♦ = deflection without logarithm
•- - - -• = power without logarithm

FIGURE IV-7

COMPARISON OF FOUR DETECTORS
FOR $P_F = 0.004$

TABLE IV-4

COMPARISON OF THE PERFORMANCE OF THE DEFLECTION DETECTOR USING A 32-POINT FFT TRANSFORM WITH ONE USING A 16-POINT TRANSFORM

Signal	$\hat{k}_{32}$	Signal $P(\hat{k}_{32})$	Noise $P(\hat{k}_{32})$	$\hat{k}_{16}$	Signal $P(\hat{k}_{16})$	Noise $P(\hat{k}_{16})$	Coherent Gain of 32 over 16	Estimated Total Gain of 32 over 16	Actual Gain P_F=0.004 P_D=0.5
A	5	84.9	60.4	3	76.1	56.6	5.0	3.5	3.5
				2	90.6	64.5	-1.6	-3.1	
B	4	95.2	65.6	3	80.5	56.6	5.7	4.2	3.5
				4	74.7	51.3	6.2	4.7	
C	8	66.2	52.7	4	58.7	51.3	6.1	4.6	4.5
				6	53.9	45.4	5.0	3.5	
D	6	94.3	56.5	3	90.0	56.6	4.4	2.9	3.0
				4	80.3	51.3	8.8	7.3	

transform at $P_D = 0.5$. Note that for the 16-point transform, the deflection detector did not always sharply distinguish a single frequency cell (partly because the simulation split the signal into two 16-point segments) which necessitated listing more than one $\hat{k}_{16}$. Except for one case, it was advantageous to use the longer FFT transform.

2. Logarithmic Transformation

We recall that the purpose of the logarithmic transformation, equation (II-4), was to 'Gaussianize' the noise and thus improve the ability of the deflection statistic $Z = (P' - \mu')/\sigma'$ to reflect signal detectability. In this instance, our intuition appears to have failed us. For the signals and noise examined, no such improvement was present. In fact, the transformation produced a slight decrease in performance. Typical results are pictured in Figure IV-7.

3. Deflection - Power Detector

As may be seen in Figure IV-5, the performance of the deflection power detector (equation (II-2)) was uniformly poorer than that of the deflection detector or power detector. This was considered somewhat surprising, and it was postulated that in a different situation (different signal and noise spectra) it might perform better. In view of the result that $S(k)/\mu^2(k)$ is an optimal filter for a power detector, i.e., for detection of a signal of known power spectrum in noise with a Gaussian power spectrum (Moll, 1974; Eckhart, 1972), it was decided to create a synthetic signal by modifying the spectrum of event D giving it the property $1/\sigma(k) = S(k)/\mu^2(k)$. As evidenced in Figure IV-8, there was a dramatic improvement. This does not, however, change the conclusion of the previous evaluation; i.e., that the deflection-power detector is not suitable for short-period seismic detection.

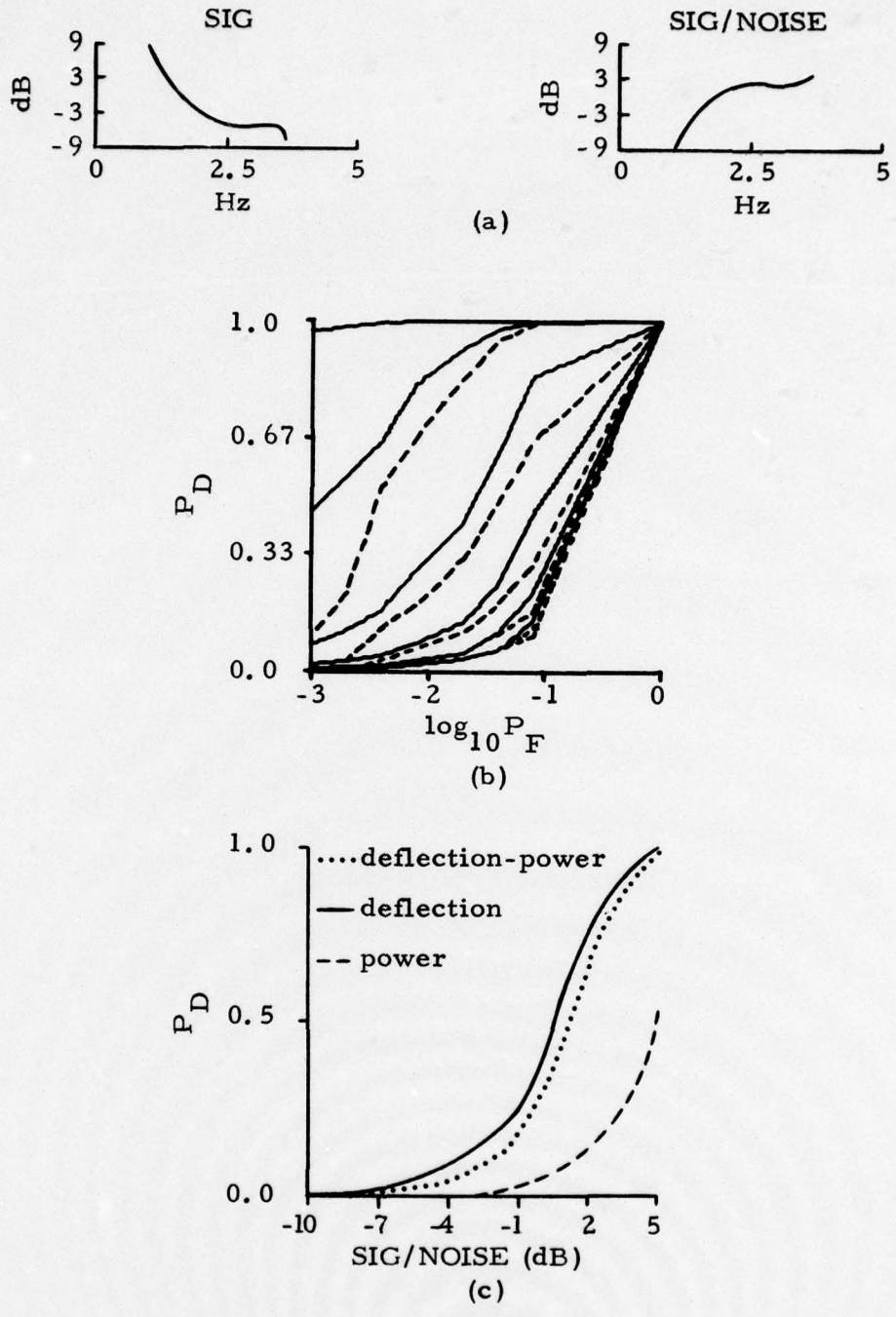

FIGURE IV-8

COMPARISON OF DETECTOR PERFORMANCE FOR SYNTHETIC SIGNAL
(a) SIGNAL AND SIGNAL-TO-NOISE RATIO SPECTRA
(b) ROC CURVES FOR DEFLECTION-POWER (SOLID)
AND POWER (DASHED) AT 3 dB INTERVALS OF SNR
(c) P_D VERSUS SIG/NOISE FOR P_F=0.004

SECTION V
CONCLUSIONS

The deflection detector and the conventional power detector shown on Figure II-1 were compared and evaluated on a set of four seismic events buried in seismic noise. The detection performance of the deflection processor was the same for one of the signals, showed a 2 dB relative loss in signal-to-noise ratio processing ability for a second signal, and a 2 dB gain for the two remaining signals. More generally, it was found that the deflection algorithm is at an advantage in detecting signals of enhanced energy content above 1.25 Hz. Such signals appear to have narrowband signal-to-noise spectra with seismic noise power concentrated at the lower frequencies. This results in greater coherent gain.

The potential usefulness of the deflection detector is perhaps better visualized in a more general setting. Figure V-1 illustrates three levels of signal information and appropriate detector configurations. Although the deflection detector possesses more versatility when the variety of signal spectra is large. For a single known signal, the ideal detector is a matched filter. However, for the detection of a whole variety of signals of diverse spectral content, the matched filter or shaped filter should be replaced by a bank of filters (one for each signal type) and a rule for deciding between signals. The deflection processor actually does this in a rudimentary manner with FFT cells used as bandpass filters. One might hope that a deflection criterion could also work at the second level shown on Figure V-1. Such a detector, for a variety of three signal spectra, is diagrammed in Figure V-2. Clearly, a crucial design factor is the determination of the number of signal types in the class to be detected and the modeling of those signals. Thus, an

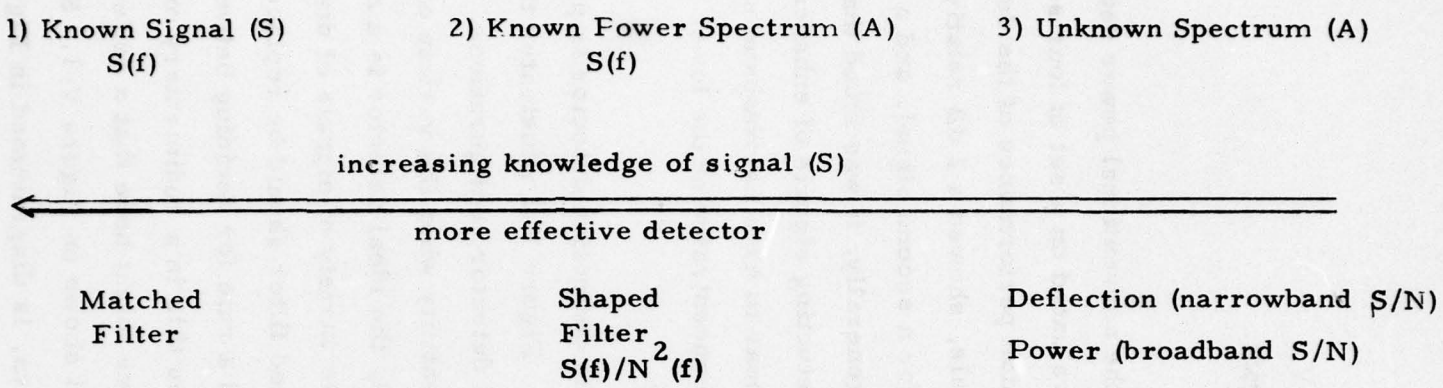

FIGURE V-1

RELATICNSHIPS BETWEEN A PRIORI KNOWLEDGE OF
SIGNAL AND DETECTOR DESIGN

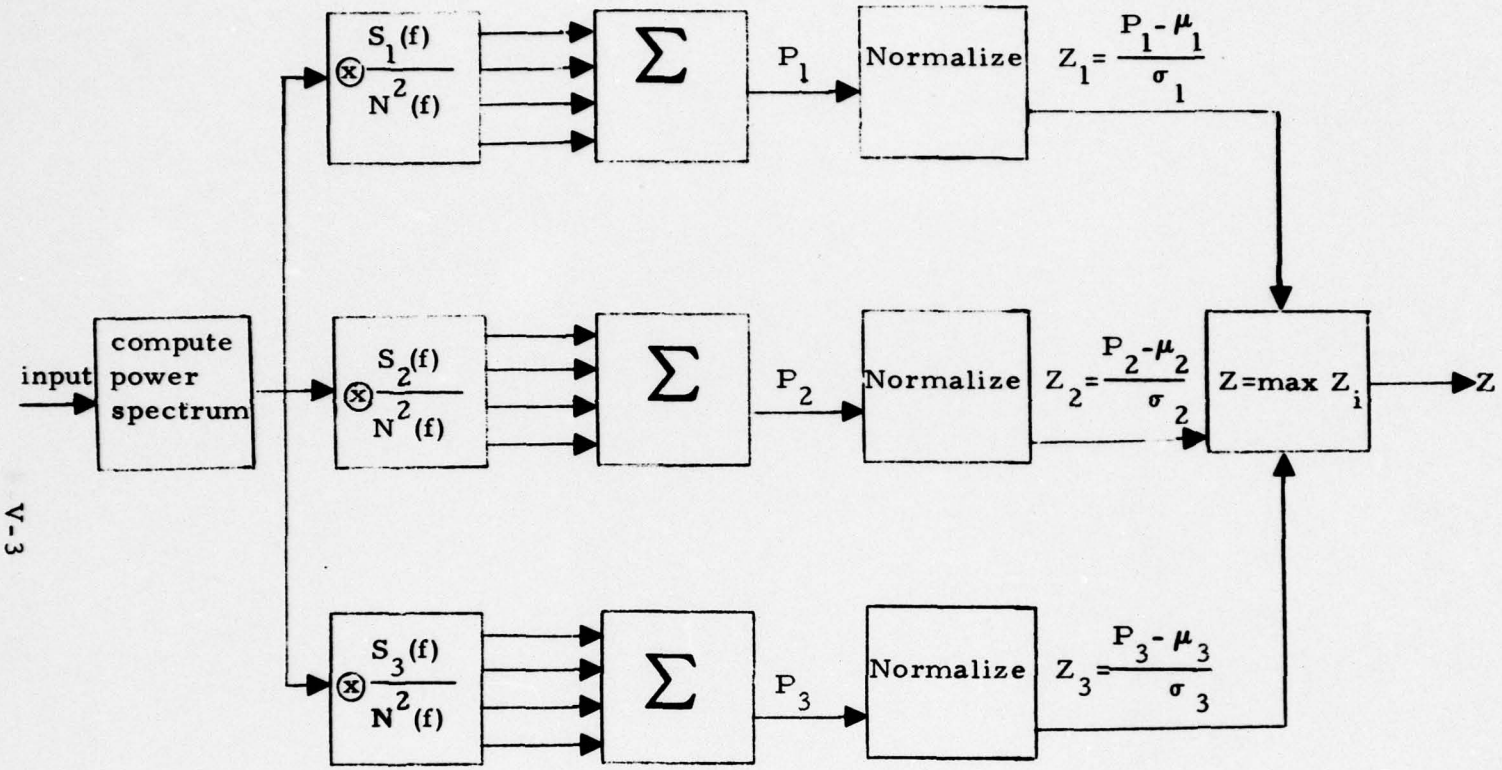

$Z = Z_j > \text{threshold} \Rightarrow \text{signal j was detected}$

FIGURE V-2

A THREE FILTER DEFLECTION PROCESSOR FOR THE DETECTION OF A CLASS CONTAINING THREE CANONICAL SIGNALS

evaluation of the usefulness of the deflection detector and/or the construction of a more powerful detector similar to that of Figure III-2 require a thorough study of the signal spectra in the region of interest and of the noise spectra.

SECTION VI
REFERENCES

Bendat, V., and A. Piersol, 1966; Measurement and Analysis of Random Data, p. 125, John Wiley, NY.

Eckhart, C., 1972; Optimal Rectifier Systems for the Detection of Steady State Signals, Scripps Inst. for Oceanography, Ref. 52-11.

Freedman, H. W., 1967; Estimating Earthquake Magnitudes, Bull. Seismol. Soc. Am., 57, 747-760.

Horton, C. W. Sr., 1969; Signal Processing of Underwater Acoustic Waves, U. S. Government Printing Office, Washington, D. C. Ch. 6, 101-115.

Hyde, D. W., and A. H. Nuttall, 1970; Square Law Detection of Narrowband Processes, NUSL Tech Memo 2020-5-70, Naval Underwater Sound Laboratory, New London, CT.

Moll, M., 1974; A Metric for Assessing the Detectability of Transient Acoustic Signals, Tech Memo W235, Bolt,Beranek and Newman, Inc.

Swindell, W. H., and N. S. Snell, 1977; Station Processor Automatic Signal Detection System, Phase I, Texas Instruments Report No. ALEX(01)-FR-77-01, Contract Number F08606-76-C-0025, Texas Instruments Incorporated, Dallas, TX.

Van Trees, H., 1968; Detection, Estimation, and Modulation Theory I, John Wiley, NY.

APPENDIX A

In many situations, it is desirable to obtain simultaneous estimates of the means and standard deviations for a large number of parameters. For example, in broadband detection several hundred frequency cells may be involved. A running average over a hundred points would require in the neighborhood of 20,000 to 50,000 words of memory. A common procedure for circumventing this difficulty is a weighted average.

$$\mu_{n+1} = (1 - \epsilon)\,\mu_n + \epsilon y_n \tag{A-1}$$

where

μ_n = estimated mean at sample n

y_n = nth sample point

$o < \epsilon < 1.$

Equation (A-1) is analogous to a RC circuit average with

$$1 - \epsilon = e^{-T/\tau} \sim 1 - \frac{T}{\tau} \sim 1 - \frac{1}{N} \tag{A-2}$$

where T is the time between samples and $\tau = RC$ is the response (averaging) time (Horton, 1969), and $\tau/T \sim N$ corresponds to the number of samples averaged.

A similar formula,

$$\sigma^2_{n+1} = (1 - \epsilon)\,\sigma^2_n + \left(\epsilon - \frac{\epsilon^2}{2}\right)(y_n - \mu_n)^2 \tag{A-3}$$

for the standard deviation involves possible pitfalls, which we proceed to discuss.

We note that the extra factor $\frac{2-\epsilon}{2}$ is introduced,

$$\beta = \epsilon - \frac{\epsilon^2}{2} = \epsilon \frac{2-\epsilon}{2} ,$$

in order that σ_n^2 be an asymptotically unbiased estimate of the variance. It corresponds to the well-known factor N/N-1 used in estimating the variance for N samples (Bendat and Piersol, 1966). More precisely, let μ and σ^2 be the true mean and variance, and define

$$\mu_\infty = \lim_{n\to\infty} E(\mu_n)$$
$$\sigma_\infty^2 = \lim_{n\to\infty} E(\sigma_n^2), \qquad \text{(A-4)}$$

which exist since the expectations of equations (A-1) and (A-3) are stable linear difference equations ($\epsilon < 1$). Taking the expectation of both sides of equation (A-1) gives

$$E(\mu_{n+1}) = (1 - \epsilon) E(\mu_n) + \epsilon\mu , \qquad \text{(A-5)}$$

so that

$$\epsilon\mu_\infty = \epsilon\mu \qquad \text{(A-5a)}$$

or

$$\mu_\infty = \mu . \qquad \text{(A-6)}$$

The square of equation (A-1) gives

$$\mu_{n+1}^2 = (1 - \epsilon)^2 \mu_n^2 + 2\epsilon (1 - \epsilon) \mu_n y_n + \epsilon^2 y_n^2 . \qquad \text{(A-7)}$$

Let

$$(\mu^2)_\infty = \lim_{n\to\infty} E(\mu_n^2).$$

Then, since μ_n and y_n are independent and $E(y_n^2) = \sigma^2 + \mu^2$, equation (A-7) yields

$$(2\epsilon - \epsilon^2)(\mu^2)_\infty = 2\epsilon (1 - \epsilon)\mu^2 + \epsilon^2 (\sigma^2 + \mu^2)$$

or

$$(\mu^2)_\infty = \mu^2 + \frac{\epsilon}{2 - \epsilon} \sigma^2 . \qquad \text{(A-8)}$$

From equation (A-3)

$$\epsilon \sigma_\infty^2 = \beta(\sigma^2 + \mu^2 - 2\mu^2 + (\mu^2))$$

$$= \beta\left(\sigma^2 + \frac{\epsilon}{2-\epsilon}\ \sigma^2\right)$$

$$= \epsilon\left(\frac{2-\epsilon}{2}\right)\left(\frac{2}{2-\epsilon}\right)\sigma^2.$$

Thus,

$$\sigma^2_\infty = \sigma^2. \tag{A-9}$$

We note that for large N (i.e., $N > 10$), ϵ is much less than one, and thus the error incurred by replacing $\epsilon - \frac{\epsilon^2}{2}$ in equation (A-3) by ϵ is negligible.

Two other candidates for recursion formulae for the variance are

$$\tilde{\sigma}^2_{n+1} = (1-\epsilon)\tilde{\sigma}^2_n + \left(\epsilon + \frac{\epsilon^2}{2-2\epsilon}\right)(y_n^2 - \mu_n^2) \tag{A-10}$$

and

$$\bar{\sigma}^2_{n+1} = (\bar{x}_{n+1} - \mu_{n+1})^2\left(1 + \frac{\epsilon}{2(1-\epsilon)}\right)$$

where

$$\bar{x}^2_{n+1} = (1-\epsilon)\bar{x}_n^2 + \epsilon y_n^2. \tag{A-11}$$

Note: σ represents the method of equation (A-3); $\bar{\sigma}$, of (A-10); and $\tilde{\sigma}$, of (A-11). None of these is biased, i.e., $\tilde{\sigma}^2_\infty = \sigma^2_\infty = \bar{\sigma}^2$; however, while the behavior of equation (A-3) and(A-11) is excellent, that of (A-10) is intolerable (see Figure A-1).

The cause of the difficulties lies in the standard deviation of the estimated variance, i.e., in

$$E(\sigma^2_{\text{estimate}} - \sigma^2)^2. \tag{A-12}$$

The quantity in (A-12) may be computed for the three recursion formulae (A-3), (A-10), and (A-11) by substituting the appropriate recursion formula

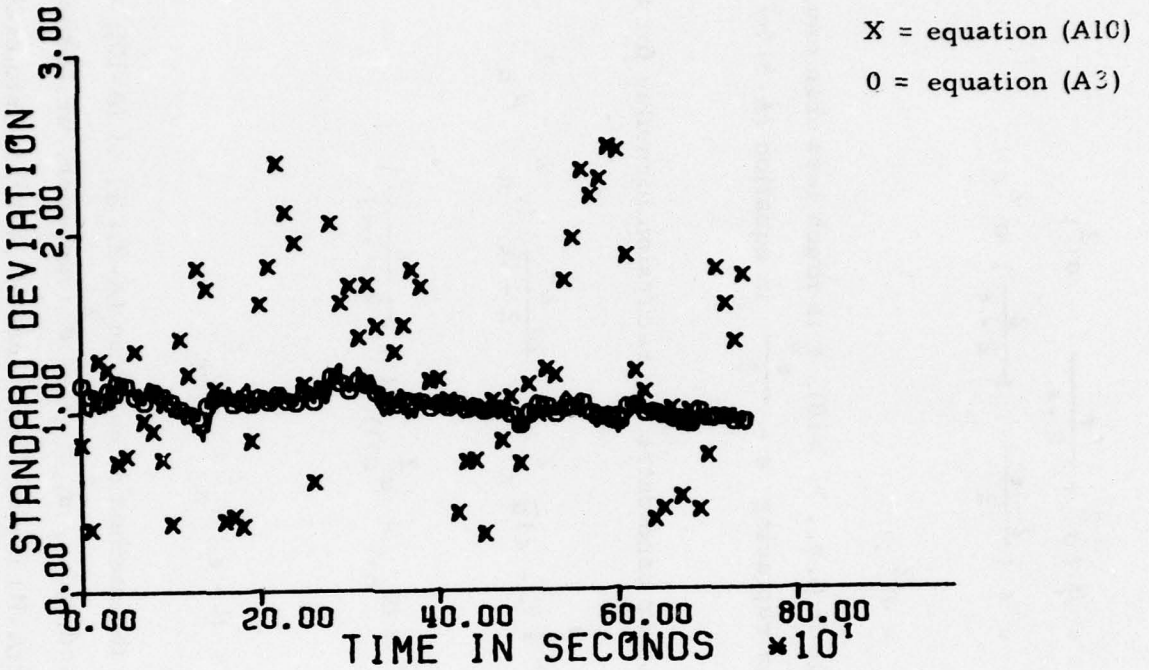

FIGURE A-1

EXAMPLE OF THE RESULTS OF TWO METHODS OF CALCULATING
THE STANDARD DEVIATION ON AN ENSEMBLE OF NORMAL PSEUDO RANDOM NOISE
(MEAN = 10, ST. DEV. = 1.0)

in (A-12) and applying the techniques used in equations (A-5) through (A-9). The algebra is extremely tedious involving the calculation of the various moments ($E(\sigma^{2\ell}$ estimate $\mu_n^k)$; $\ell = 0, 1, 2$, and $k = 0, \ldots, 4$) and thus only the final expressions will be presented. To the first order in ϵ, we have

$$E(\sigma_\infty^2 - \sigma^2)^2 = \epsilon \left[\frac{G - \sigma^4}{2}\right] \tag{A-13}$$

$$E(\tilde{\sigma}_\infty^2 - \sigma^2)^2 = \epsilon \left[\frac{G - \sigma^4}{2} + 2\mu B + \sigma^2\mu^2\right] \tag{A-14}$$

$$E(\bar{\sigma}_\infty^2 - \sigma^2)^2 = \epsilon \left[\frac{G - \sigma^4}{2}\right] \tag{A-15}$$

where $B = E(y_n - \mu)^3$ and $G - E(y_n - \mu)^4$ are the third and fourth central moments of the distribution (assumed stationary), respectively. For the Gaussian case, these may be simplified:

$$E(\sigma_\infty^2 - \sigma^2)^2 \sim \epsilon\sigma^4 \tag{A-16}$$

$$E(\tilde{\sigma}_\infty^2 - \sigma^2)^2 \sim \epsilon(\sigma^4 + \sigma^2\mu^2) \tag{A-17}$$

$$E(\bar{\sigma}_\infty^2 - \sigma^2)^2 \sim \epsilon\sigma^4 \,. \tag{A-18}$$

For small ϵ (i.e., large N) the formulae (A-16) to (A-18) are quite accurate. A comparison between the values computed by (A-16) and (A-18) with the exact values for the Gaussian case appear in Figure A-2. It follows from equations (A-13) through (A-15) that $\bar{\sigma}^2$ and σ^2 have comparable behavior and are always better than $\tilde{\sigma}^2$. In general, for small values of $\frac{\mu^2}{\sigma^2}$, all three will give similar results; however, for $\mu^2 << \sigma^2$, the variance of σ_∞^2 and $\bar{\sigma}_\infty^2$ will be of the same order, whereas that of $\tilde{\sigma}_\infty^2$ will be much larger. This explains the erratic behavior observed in Figure A-1.

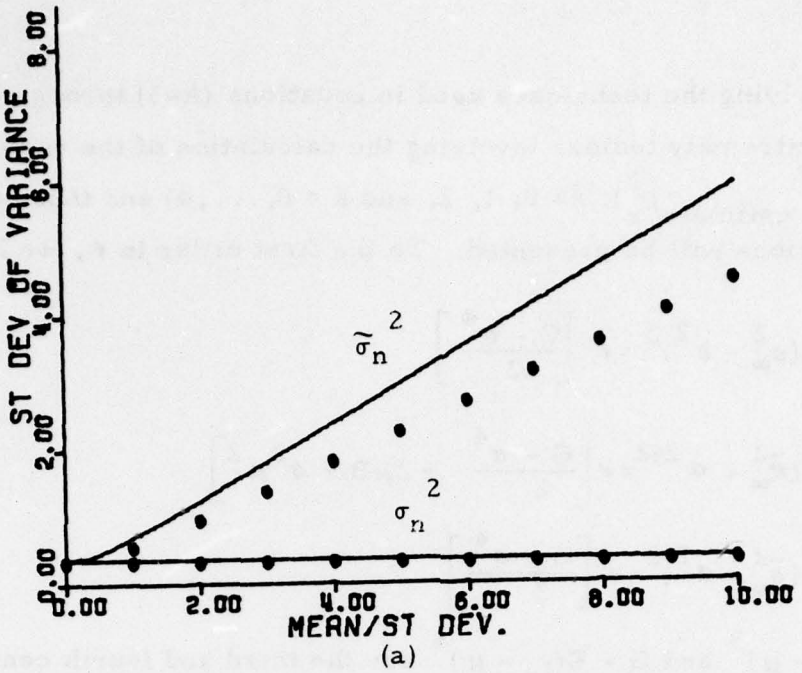

(a)

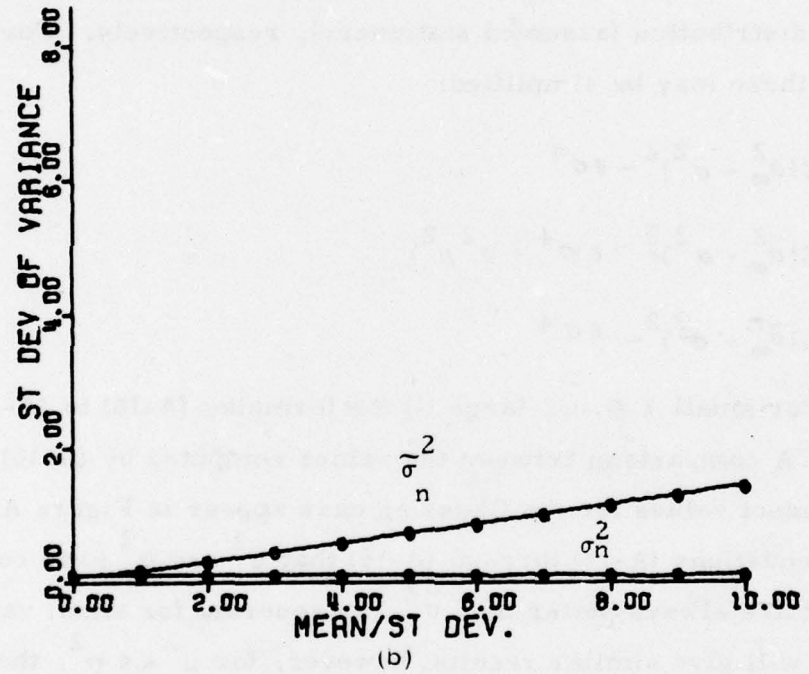

(b)

FIGURE A-2

GRAPHS OF THE STANDARD DEVIATION OF THE ESTIMATED VARIANCE VERSUS THE RATIO OF MEAN TO STANDARD DEVIATION FOR GAUSSIAN DISTRIBUTIONS FOR (a) $\epsilon = 0.2$ AND (b) $\epsilon = 0.02$. THE SOLID LINES REPRESENT THE TRUE VALUE AND THE O'S REPRESENT THE APPROXIMATIONS OF (A16) TO(A18)